Importance of excited bound states in harmonic generation

Carla Figueira de Morisson Faria,[1] Martin Dörr,[1,2] and Wolfgang Sandner[1]
[1]*Max-Born-Institute, Rudower Chaussee 6, 12474 Berlin, Germany*
[2]*Physique Théorique, Code Postal 227, Université Libre, B-1050 Bruxelles, Belgium*
(Received 12 March 1998)

We discuss the mechanism of harmonic generation for a one-dimensional model atom with several bound states in a strong, driving laser field. We extract the bound- and continuum-components of the harmonic radiation and investigate their temporal and spectral characteristics. We compare the bound-bound contributions from a fully numerical solution of the Schrödinger equation with the results from a two-level atom, and study the influence of effective ionization rates in the latter. In the generation of the low harmonics, bound-bound transitions play a decisive role. However, a two-level atom model is not adequate for reproducing their characteristics. High-harmonic generation is almost entirely determined by bound-continuum transitions, the transitions involving the ground state being dominant. [S1050-2947(98)11009-0]

PACS number(s): 32.80.Rm

I. INTRODUCTION

Radiation of high harmonics from atoms driven by strong laser fields is at present a subject of growing interest, mainly for the potential applications of the emitted tunable, short-pulse, high-brilliance, coherent, high-frequency radiation. The atomic process of high-harmonic generation (where ''high'' means more than 10th order and up to over 100th order) is at present modeled most successfully by a ''three-step'' physical picture [1–3]. This model explains most of the experimentally observed spectral features [4], namely the extended ''plateau'' consisting of many harmonics with comparable intensities, and its sharp high-frequency ''cut-off,'' which are clearly in contradiction with perturbative theories concerning the external laser field. Within this picture, the ''first step'' is ionization, the ''second step'' is propagation of the free electron in the laser field, and the ''third step'' is the collision between the returning electronic wave packet driven by the external laser field and the atomic core potential. The result of this collision is harmonic generation. Around this main idea [1], three-step theoretical models for harmonic generation were developed [2,3], where just a single-bound-state atom is taken into account, thus neglecting transitions between atomic bound states. The predicted maximum energy of the harmonics at the ''cutoff'' is $\varepsilon_{\mathrm{cutoff}}=|\varepsilon_0|+3.17U_p$, which corresponds to the maximal quasiclassical rescattering energy of the electron, $|\varepsilon_0|$ being the ionization potential and U_p the ponderomotive energy.

However, harmonic spectra can also be described within a completely different physical picture, namely a driven two-level atom [5,6], for which bound-continuum transitions do not exist. Recently, however, the inclusion of a ''three-step-like'' recombination mechanism in the bound-state populations of a two-level atom was able to reproduce a plateau and sharp cutoff at $\hbar\omega_{10}+3.17U_p$, where $\varepsilon_1-\varepsilon_0=\hbar\omega_{10}$ is the energy difference [7].

In the present paper, we address the question of whether the two pictures of rescattering and bound-level transitions can be compatible and what are their respective ranges of applicability concerning harmonic generation, for atoms with several bound states. The goal of these studies is to gain some insight in the process of generation of harmonics when several bound states are involved, and to include information about their phase (in other words, the complementary temporal structure of the harmonics), with the eventual aim of being able to control this emission for tailoring harmonic pulses of desired characteristics. The atomic harmonic generation results are the basis of further computations of the propagation of harmonic radiation: phase matching is most sensitive on the intensity dependence of the emitted atomic harmonics [8]. The models we consider have been and are widely used in such propagation studies [9]: although a 1D atom does not yield quantitatively accurate rates, it contains the essential physics of the problem (in linearly polarized laser light). We base our discussion on the fully numerical solution of the time-dependent Schrödinger equation, which we regard as the full, ''benchmark'' solution. This approach has the advantage that it includes all bound-bound, bound-continuum, and continuum-continuum transitions, thus incorporating time-dependent effects such as ground- and excited-state depletion, ionization, and recombination. As a first step we must define and isolate the different mechanisms and investigate their contribution to harmonic generation. To first approximation, we project the time-dependent wave function onto the field-free bound states, the remainder being an effective time-dependent continuum.

Using spectral and time-frequency analysis, we perform a detailed investigation of the radiation emitted by the atom. The case of a system with two bound states and a continuum is investigated in detail and compared with a two-level atom model. In previous work [10] we considered the case of an atom with a *single* bound state. We used time-frequency analysis in order to compare the fully time-dependent solution of the Schrödinger equation with the three-step model [2]. The time profiles of the plateau and cutoff harmonics were strikingly similar for both models, corresponding to the semiclassical return times for the electronic wave packet. In the present case, however, for an atom supporting more than one field-free bound state, such a coincidence is not always observed, especially for the lower order plateau harmonics.

The paper is organized as follows: in Sec. II we discuss the theoretical methods used, namely the time-dependent projections, the wavelet transform, and a two-level atom model with and without ionization. In Sec. III we present our

results. We have taken several model potentials to investigate two bound states in a short-range potential (Sec. III A), one deeply bound and many weakly bound states in a long-range (soft Coulomb) potential (Sec. III B), several deeply bound (and many weakly bound) states in a deep soft-Coulomb potential (Sec. III C), and the same potential as in Sec. III C, but with its Coulomb tails cut off (Sec. III D). In Sec. IV we state our conclusions.

II. THEORETICAL METHODS

A. Fully time-dependent projections

As our point of reference we take a fully time-dependent numerical computation, solving the Schrödinger equation for a one-dimensional model atom in a time-dependent external laser field. We consider both short- and long-range potentials supporting more than one field-free bound state. The one-dimensional case is particularly interesting and widely used for modeling harmonic generation in linear polarization [11], since it requires much less computer time than three-dimensional computations, being therefore amenable to an expedient, and accurate numerical solution. Furthermore, the use of a short-range potential implies a very good applicability for three-step models.

We use atomic units throughout. The time propagation is performed in the velocity gauge, using the standard finite-difference Crank-Nicolson method. The time-dependent Hamiltonian is

$$H=\frac{p^2}{2}-pA(t)+V(x). \tag{1}$$

The vector potential of the driving laser field is in the dipole approximation $A(t)=\overline{A}(t)\cos(\omega_L t)$, with $\overline{A}(t)$ its envelope. The electric field is then $E(t)=-dA(t)/dt$. In Eq. (1) the purely time-dependent phase term $A^2(t)$ has been eliminated through a unitary transfomation. The emission spectrum is taken to be proportional to the modulus square of the Fourier transform of the dipole acceleration, which is calculated using Ehrenfest's theorem [12]. The dipole acceleration operator is

$$\ddot{\hat{x}}=-\frac{dV(x)}{dx}+E(t). \tag{2}$$

The time-dependent wave function $|\psi(t)\rangle$ can be expanded into the field-free-bound-state basis

$$|\psi(t)\rangle=\sum_n C_n(t)|n\rangle+|\phi_c(t)\rangle, \tag{3}$$

where the bound states are denoted by $|n\rangle$, the remaining continuum part of the wave function by $|\phi_c(t)\rangle$ and $C_n(t)=\langle n|\psi(t)\rangle$. The average dipole acceleration $\ddot{x}(t)=\langle\psi(t)|\ddot{\hat{x}}|\psi(t)\rangle$ can therefore be split into

$$\langle\psi(t)|\ddot{\hat{x}}|\psi(t)\rangle=\ddot{x}_{bb}(t)+\ddot{x}_{bc}(t)+\ddot{x}_{cc}(t), \tag{4}$$

with the bound-bound, bound-continuum, and continuum-continuum contributions being, respectively,

$$\ddot{x}_{bb}(t)=\sum_{n,m} C_m^*(t)C_n(t)\left\langle m\left|\frac{-dV(x)}{dx}\right|n\right\rangle + E(t)\sum_n |C_n(t)|^2, \tag{5}$$

$$\ddot{x}_{bc}(t)=\sum_n 2\,\mathrm{Re}\left[C_n(t)\left\langle\phi_c(t)\left|\frac{-dV(x)}{dx}\right|n\right\rangle\right], \tag{6}$$

and

$$\ddot{x}_{cc}(t)=\langle\phi_c(t)|\ddot{\hat{x}}|\phi_c(t)\rangle. \tag{7}$$

The $E(t)$ term in Eq. (2) contributes only to an enhancement in the fundamental in the spectrum of the full acceleration. However, for the bound-bound and continuum-continuum contributions (4) and (6), there is a somewhat artificial introduction of a term proportional to the field. This term does, however, not introduce any important contributions, as will be shown in Sec. III.

It should be noted that each term of the expansions above is in general not invariant under unitary transformations. This can be easily verified by applying a transformation Ξ on $|\psi(t)\rangle$, such that the wave function in the new representation is written as $|\psi_\Xi(t)\rangle=\Xi|\psi(t)\rangle$. For the amplitudes $C_n(t)$ one obtains

$$C_{n\Xi}(t)=\sum_{j=0}^{n}\langle n|\Xi|j\rangle C_j(t)+\langle n|\Xi|\phi_c(t)\rangle, \tag{8}$$

with the continuum being

$$|\phi_{c\Xi}(t)\rangle=|\psi_\Xi(t)\rangle-\sum_n C_{n\Xi}(t)|n\rangle. \tag{9}$$

The nondiagonal terms correspond to couplings between different basis states introduced by the transformation. If these couplings are zero, Eq. (8) is diagonal and therefore each contribution to the time-dependent spectra remains invariant. This is the case of, for instance, purely time-dependent transformations. Under gauge transformations, for instance $\Xi=e^{-ixA(t)}$ (from the velocity gauge to the length gauge), the nonzero couplings can lead to different results [13]. Particularly in the velocity gauge, we could observe unphysical behavior for the amplitudes $C_n(t)$. Therefore we always performed the transformation to the length gauge before calculating our projections numerically. The misleading results obtained using the velocity gauge are presented and discussed in Sec. III E. Obviously, the expansion into a *field-free* bound-state basis yields just an approximate picture for the bound-state subspace, since in a real atom the higher excited bound states are strongly distorted by the field and coupled to the continuum. Moreover, the projections $\langle\psi(t)|n\rangle\langle n|\ddot{\hat{x}}|m\rangle\langle m|\psi(t)\rangle$ are *not* equivalent to the respective second temporal derivatives of the dipole length projections, $d^2\langle\psi(t)|n\rangle\langle n|\hat{x}|m\rangle\langle m|\psi(t)\rangle/dt^2$, since the projection operators $|n\rangle\langle n|$ do not commute with the full Hamiltonian (1). Therefore, for an atom with two bound states, a direct comparison between $\ddot{x}_{bb}(t)$ of Eq. (5) and the dipole acceleration of a two-level atom is questionable. This error is not introduced if we compare the bound-bound projections and

the two-level atom dipole in the length form, used as a test in Sec. III A.

B. Two-level atom

We shall address now the driven two-level atom case, with and without ionization, with the objective of comparing the power spectra obtained in this physical picture with the bound-bound contributions from the full 1D atom, as discussed in the preceding subsection. For a ''closed'' (nonionizing) two-level atom in an external field $E(t)$, the time-dependent wave function and Hamiltonian are given, respectively [14], by

$$|\psi(t)\rangle = C_0(t)|0\rangle + C_1(t)|1\rangle \tag{10}$$

and

$$H = H_A + H_I . \tag{11}$$

The amplitudes $C_n(t)$, $n=0,1$ are $C_n(t)=\langle n|\psi(t)\rangle$, as defined in the preceding section. The indices 0 and 1 relate, respectively, to the ground and excited state. The atomic Hamiltonian is

$$H_A = |0\rangle\varepsilon_0\langle 0| + |1\rangle\varepsilon_1\langle 1|, \tag{12}$$

with ε_n the field-free energies, such that $H_A|n\rangle = \varepsilon_n|n\rangle$. The atom-field interaction is represented by

$$H_I = -x_{10}E(t)(|1\rangle\langle 0| + |0\rangle\langle 1|), \tag{13}$$

x_{10} being the matrix element $\langle 1|x|0\rangle$. The dipole moment and acceleration operators are given, respectively, by

$$\hat{x}_{TL} = x_{10}(|1\rangle\langle 0| + |0\rangle\langle 1|) \tag{14}$$

and

$$\ddot{\hat{x}}_{TL} = -\omega_{10}^2\hat{x}_{TL} + 2\omega_{10}x_{10}^2E(t)(|0\rangle\langle 0| - |1\rangle\langle 1|), \tag{15}$$

with the energy difference $\omega_{10}=\varepsilon_1-\varepsilon_0$. The amplitudes $C_n(t)$ are the solution of the following system of coupled differential equations:

$$i\frac{d}{dt}\begin{pmatrix} C_0 \\ C_1 \end{pmatrix} = \begin{pmatrix} \varepsilon_0 & x_{10}E(t) \\ x_{10}E(t) & \varepsilon_1 \end{pmatrix}\begin{pmatrix} C_0 \\ C_1 \end{pmatrix}. \tag{16}$$

We solved Eq. (16) numerically using a standard fourth-order Runge-Kutta method.

Introducing now ionization [6,15], we choose an atom with a ground state in the tunneling ionization regime and the excited state in the over-the-barrier ionization regime, with time-dependent ionization rates, respectively, $\gamma_0(t)$ and $\gamma_1(t)$. The ground-state ionization rate was chosen as the quasistatic tunneling formula [16] for the one-dimensional case

$$\gamma_0(t) = D_1\exp(-D_2/|E(t)|), \tag{17}$$

where D_1 and D_2 are positive real parameters. For the excited state we took

$$\gamma_1(t) = D_3\ \exp(-D_4/|E(t)|^2), \tag{18}$$

where D_3 and D_4 are adapted as discussed in Sec. III. Equation (16) will now be solved with the energies ε_n replaced by the complex quantities $\tilde{\varepsilon}_n = \varepsilon_n - i\gamma_n(t)/2$. Harmonic generation is due to transitions involving the time-dependent dressed states, whose energies are obtained by diagonalizing the Hamiltonian (11). The instantaneous transition frequency between these dressed levels is given by

$$\omega_{01D}(t) = (\{\varepsilon_0-\varepsilon_1 - i[\gamma_0(t)-\gamma_1(t)]/2\}^2 + 4x_{01}^2E(t)^2)^{1/2}. \tag{19}$$

The cutoff frequency is the maximal value of $\mathrm{Re}[\omega_{01D}(t)]$ [5,6]. The energy width introduced by ionization in principle can cause an increase in the cutoff frequency. Furthermore, harmonics can be generated by the nonlinearity introduced by the functional forms of γ_0 and γ_1.

C. Fourier and wavelet analysis

By calculating the power spectra, all the temporal information about harmonic generation is lost. Certain features of harmonic generation that are present in, for instance, three-step models [17] can only be revealed by a time-frequency analysis. Several groups [9,10,21] have employed time-resolved spectra for analyzing the time dependence of harmonic generation. These spectra are obtained by performing a Fourier transform with a temporally restricted envelope. We choose the time width of the window function narrower than a period of the external laser field. In this way the contribution from a particular group of harmonics to the emitted radiation can be determined. This procedure differs slightly from the time-frequency analysis performed by most groups [9,21], which take this width larger than the laser period $T=2\pi/\omega_L$ in order to investigate the time profile of a single specific harmonic. In principle, the harmonic generation process is almost periodic, with the period of the driving laser frequency, or rather with half this period. This periodicity is observed only approximately in the results that follow, due to turn-on transient and ionization effects in the actual computation.

We perform a wavelet transform with a Gaussian window function (Gabor transform), which is given by

$$W(t,t',\Omega,\sigma) = \exp[-(t-t')^2/\sigma^2]\exp[i\Omega t'], \tag{20}$$

of width σ and centered at a harmonic frequency $\Omega = N\omega_L$. The wavelet transform of a function $f(t)$ is defined as

$$\mathcal{W}(t,\Omega,\sigma) = \int_{-\infty}^{+\infty} dt' f(t')W(t,t',\Omega,\sigma). \tag{21}$$

The usual Fourier transform, in which all temporal information is lost, is obtained for $\sigma\to\infty$. Just as for the time-dependent dipole in Sec. II A, one can split the time-dependent power spectra into the corresponding bound-bound, bound-continuum, and continuum-continuum contributions. We thus obtain the wavelet transform of the dipole acceleration (4) and its projections,

$$\begin{aligned}|\mathcal{W}(t)|^2 = {} & |\mathcal{W}_{bb}(t)|^2 + |\mathcal{W}_{bc}(t)|^2 + |\mathcal{W}_{cc}(t)|^2 \\ & + 2\mathrm{Re}\{\mathcal{W}_{bb}(t)\mathcal{W}_{bc}^*(t) + \mathcal{W}_{bc}(t)\mathcal{W}_{cc}^*(t) \\ & + \mathcal{W}_{bb}(t)\mathcal{W}_{cc}^*(t)\},\end{aligned} \tag{22}$$

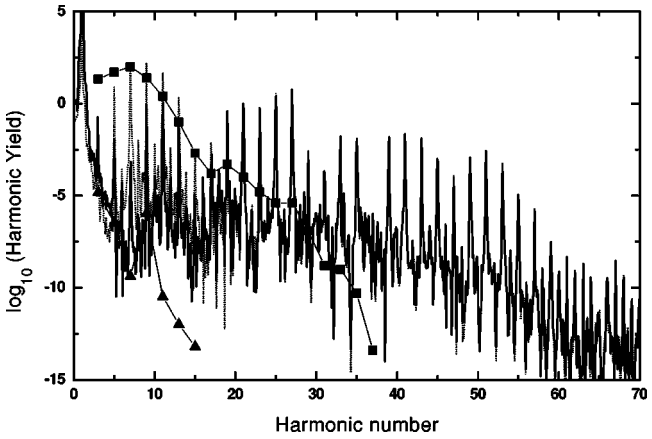

FIG. 1. Power spectra for the short-range Gaussian potential (23) and its two-level atom model. Dotted line: full acceleration; solid line: bound-continuum part; squares: bound-bound part; triangles: two-level atom including ionization (for the latter two, only the harmonic peak heights are shown, connected by a thin line).

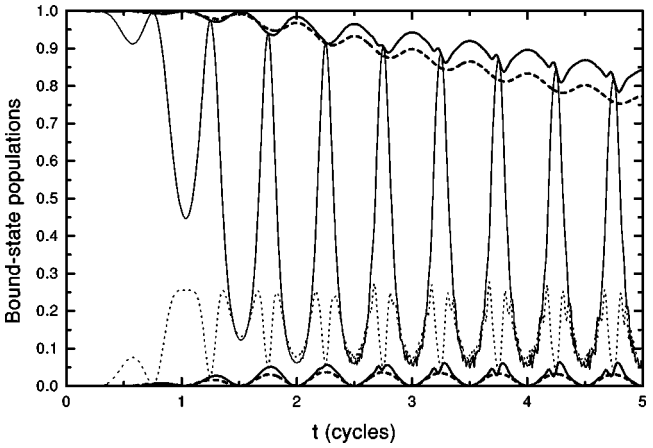

FIG. 2. Bound-state populations. Solid heavy lines: full time-dependent computation for the short-range Gaussian potential. Dashed heavy lines: two-level atom with ionization. Solid and dotted light lines: full time-dependent calculation with projections in the velocity gauge (See III E). The upper curves are for the ground state, the lower ones for the excited state.

where not only the separate contributions but also their relative phases play an important role, since there are crossed terms.

III. RESULTS AND DISCUSSION

A. Short-range potential

In order to test the two-level atom against the fully time-dependent solution of the Schrödinger equation, we chose a Gaussian short-range potential

$$V_G(x) = -0.76 \exp(-x^2/4). \tag{23}$$

This potential supports two field-free bound states, at $\varepsilon_0 = -0.499$ a.u. and $\varepsilon_1 = -0.099$ a.u. We consider an external field of frequency $\omega_L = 0.05$ a.u. and amplitude $E_0 = 0.08$ a.u., which is clearly in the tunneling regime for the ground state. These conditions are comparable to the ones considered in [6], i.e., ground state in the tunneling regime, excited state in the over-the-barrier regime, and dipole matrix element $\langle 0|x|1\rangle = 1.066$ a.u. According to the three-step models, the expected cutoff for the present case should be at $\Omega = 49\omega_L$, which is in very good agreement with the spectrum for the full acceleration, shown as the dotted line in Fig. 1. In fact, the dotted line beyond the harmonic 21 superposes exactly on the solid line, which gives only the bound-continuum part of the spectrum, resulting from $\ddot{x}_{bc}(t)$, Eq. (6). At low energy the bound-continuum part underestimates the full results, while the bound-bound part gives the dominant contribution. The bound-bound spectrum presents a completely different cutoff (at roughly $\Omega = 35\omega_L$) and no clear indication of a plateau, in contrast to the full dipole acceleration.

In order to verify whether these features correspond to a two-level atom, we compare the bound-bound part with the corresponding two-level atom, with and without ionization. Without taking ionization into account, we do not observe a plateau structure at all in the emission spectra for the field parameters above. In fact, the only peaks observed correspond to the fundamental, a few very weak harmonics (up to the 5th), and the resonance peak around the transition $|0\rangle \rightarrow |1\rangle$. Harmonic spectra with an extended plateau structure are only observed for much higher intensities, where any real atom would ionize practically instantaneously and the two-level atom description is unrealistic. These results are not shown in the figure.

As a further step, we introduce ionization rates for the bound-state populations as stated in Sec. II B. The tunnel formula for the ground state yields $D_1 = 0.72$ and $D_2 = 0.665$ in Eq. (17). For the excited state we choose $D_3 = 0.05$ and $D_4 = 0.0026$ in Eq. (18). The harmonic spectrum obtained in this case is very different from the full solution spectrum or from the bound-bound part of the full solution. Harmonics up to the 9th are visible, which is in agreement with Eq. (19), but these harmonics are much weaker than those of the full result. We conclude that the driven two-level atom is not a good model for computing the harmonic response, not even for the low harmonics, which can be extracted as the bound-bound part of the spectrum. A strongly nonlinear ionization rate within the two-level atom model can enhance the harmonics and prolong the plateau, but then the field-dependent ionization rate does not reproduce the full solution's time dependence for the populations of the bound states, obtained by the time-dependent projection onto the unperturbed states, shown in Fig. 2. Actually, the rate $\gamma_1(E(t))$ of Eq. (18) for the excited state is just an ad hoc adjusted quantity since a tunnel formula is not too appropriate for this state whose binding energy $\varepsilon_1 = -0.099$ a.u. is only $2\hbar\omega_L$. Choosing a step function as a model of the over-the-barrier ionization process yields more harmonics since it is more nonlinear [6], but it is arguably less realistic.

The ground- and excited-state populations depicted in Fig. 2 show reasonably similar behavior for the full solution and the two-level atom model. The excited-state population of the full solution is quasiperiodic in time, with a zero at the times for which the field is zero. There are small dips (after the second cycle) at the times for which the field is maximal. The small dips in the excited-state population are mirrored by corresponding peaks in the ground-state population These

dips, which are absent in the two-level atom results, are an indication that a nonlinear process is taking place around the peak field intensity, which involves just the two bound states. Both the full and the two-level atom calculations contain irreversible ionization, partially over-the-barrier ionization, the excited state having the function of an intermediate state between the ground state and the continuum, and partially tunneling ionization. It must be noted that, even though recombination is present in the bound state part of the time evolution for the full results, the bound-bound part of the spectrum in Fig. 1 does not exhibit the cutoff at $\omega_{10}+3.17U_p$ observed by [7].

The time-frequency wavelet gives a more detailed analysis of the harmonic generation process, including in part the harmonics' phase information. In Figs. 3(a)–3(d), we present results obtained for low harmonics taking a time width $\sigma=0.1T$. In Fig. 3(a), we plot the wavelet transform for $\Omega=7\omega_L$. In this case, the main contribution to harmonic generation within a field cycle for the full solution occurs close to the field peak. The full and the bound-bound contributions have very similar shapes, the same amplitudes, and coincident peaks. However, the bound-bound wavelet transform of the fully time-dependent computation and the two-level atom wavelet transform are remarkably different. The two-level atom results exhibit peaks at $t=0.5T$ modulo $T/2$, that is, when the field $E(t)$ is zero. The full or the bound-bound results have also a small shoulder at $t=0.5T$ mod $T/2$, but their main peak is 90° out of phase with the two-level-atom results, being at $t=0.25T$ mod $T/2$. In order to test whether this discrepancy is introduced by the fact that the projection operators onto the bare bound states do not commute with the full Hamiltonian (1), we performed the same calculation using the bound-bound projections and the two-level atom dipole, both in the *length* form; the result is shown in Fig. 3(b). The bound-bound contributions from the full solution in the length and acceleration forms in parts (a) and (b) exhibit peaks at the same times. This shows that the error introduced by the fact that $[|n\rangle\langle n|,H]\neq 0$ is of no qualitative importance in this situation. Once more, the two-level atom results in part (b) present peaks at times different from the x_{bb}. The shape and location of the peaks obtained for the two-level atom are not sensitive to variations in the ionization rates γ_0 and γ_1.

These results, together with the large difference in the magnitude of the harmonics, visible in Fig. 1, strongly suggest that the process of generation of these low harmonics must be quite different in the two cases, even though the full results are recovered in their two-bound-state projections. The generation of harmonics within the two-level-atom model has been investigated by Gauthey *et al.* [18]. They conclude that harmonics occur due to a crossing between the two dressed states. The wavelet transform for the parameters used in [18] exhibits indeed well-localized sharp peaks at $t=0.5T$ mod $T/2$. In our present case, however, the time width of the avoided crossing between the two dressed levels becomes comparable to (although still smaller than) the laser field period and thus the peaks are no longer so sharp. For the full 1D atom results, on the other hand, the field is driving the bound part of the electronic wave packet primarily within the two lowest bound states, as can be seen in Fig. 2 (the slow decrease in the ground-state population is due to irreversible ionization). Since the frequency is low, the wave packet follows adiabatically the Stark eigenstate of the potential, which is distorted by the slowly time-varying electric field. The largest field gives rise to the largest dipole and also to the largest harmonic components in this dipole. The generation of harmonics of the bound part can also be viewed as arising from a ''charge oscillation'' of the wave packet between dipoles of opposite parity in the atom. The same mechanism leads to even more dramatically visible effects in the emission of harmonics from a diatomic molecule when considering the two lowest bound even- and odd-parity states [19,20]. Classically, an electron driven by the field over a few a.u. (the spatial extension of the bound states) will gain the largest energy when the field is largest. This suggests that the harmonics generated by this process should occur around the peak of the field $E(t)$, an observation that is also in accord with a calculation of the phase, for the molecular case [20]. The small but sharp peaks close to maximum field observed in the full solution populations (Fig. 2) are a further evidence for this mechanism. The time between the two small peaks in the excited-state population, of about 10 a.u.,

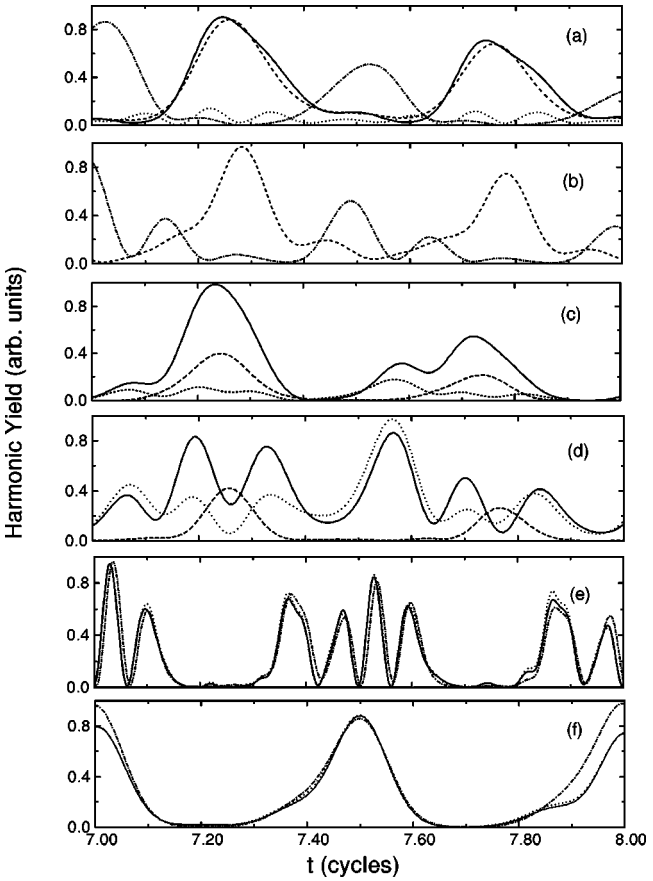

FIG. 3. Wavelet analysis of the time-dependent dipole over one cycle of the driving laser field for the short-range Gaussian potential. (a) and (c)–(f) give the dipole acceleration, whereas (b) gives the dipole length. (a) and (b) $\Omega=7\omega_L$, $\sigma=0.1T$; (c) $\Omega=15\omega_L$; (d) $\Omega=17\omega_L$; (e) $\Omega=37\omega_L$, $\sigma=0.024T$ (plateau harmonics); (f) $\Omega=49\omega_L$, $\sigma=0.1T$ (cutoff harmonics). Solid line: full dipole acceleration. Dashed line: bound-bound contributions. Dotted line: bound-continuum contributions. Dotted-dashed line: in (a) and (b) results from the two-level atom with ionization (multiplied by 3000); in (e) and (f) continuum-ground-state contributions.

is equal to the time it takes for a classical particle to be accelerated by the field from rest to a distance corresponding to the shift of the charge cloud at peak field. In our model, we observed a related spatial displacement in the peak of the probability distribution of the bound-state part of the wave function, $|\psi_b(t)\rangle = C_0(t)|0\rangle + C_1(t)|1\rangle$, which occurs roughly within this time interval. It is only a small part of the wave packet that performs this motion (while the majority simply follows the field adiabatically) but this is the significant part producing the lower plateau harmonics. This mechanism is not taken into account in the two-level-atom model.

Considering now the wavelet transform centered at the low-frequency end of the plateau harmonics, $\Omega = 15\omega_L$, shown in Fig. 3(c), one observes that the full wavelet has significant contributions from both the bound-continuum and the bound-bound parts. Increasing the center wavelength just slightly, to $\Omega = 17\omega_L$, the bound-bound part rapidly loses its importance. In Fig. 3(d), the bound-continuum and the full wavelet almost coincide, the bound-bound contributions now being out of phase with the full solution. Thus the dominant contribution in the full results shifts from the bound-bound part for the low harmonics to the bound-continuum part, over just a few harmonics, as is evident also from Fig. 1.

Finally, in Figs. 3(e) and 3(f) we analyze the plateau and cutoff regions. In Fig. 3(e), we consider a window function of time width $\sigma = 0.024T$ centered at $\Omega = 37\omega_L$, so that most of the plateau harmonics are included. For this situation, we observe a near-perfect coincidence between the bound-continuum (dotted line) and the full (solid line) results, in accord with the results in Fig. 1. The main contributions to the bound-continuum part come from the ground-state-continuum transition (dotted-dashed line).

Fig. 3(f) shows the wavelet transform for the cutoff harmonics, $\Omega = 49\omega_L$, with time width $\sigma = 0.1T$. Here the full result and the contributions involving the ground-state-continuum transitions (dotted-dashed line) and the bound-continuum transitions $\ddot{x}_{bc}(t)$ are almost identical. The peak in part (f) corresponds to the classical return time of an electron with maximum kinetic energy (see, e.g., [17] or [10] and references therein). We observed small variations in the position of this peak between $t = 0.4T$ and $t = 0.5T$, which is reasonable since this return time is very sensitive towards small variations in the electron energy, as discussed in [17]. For all cases, the continuum-continuum transitions yield very small contributions, in accord with the analysis of [22].

B. Shallow long-range potential

In the following two subsections, in order to investigate the influence of the potential shape on harmonic generation, we consider model atoms with the widely used soft Coulomb potential

$$V_C(x) = -\alpha[(x/\beta)^2 + 1]^{-1/2}. \tag{24}$$

We take $\alpha = 0.38$ and $\beta = 0.76$, which leads to one bound state of energy $\varepsilon_0 = -0.19$ a.u. and several weakly bound states (binding energies of the order of 10^{-2} a.u. and smaller) in an external field of amplitude $E_0 = 0.08$ a.u. and frequency $\omega_L = 0.05$ a.u. This case is very close, apart from the potential shape, to the single-bound-state short-range potential discussed in [10], since in the presence of the external field the excited states are strongly coupled to the continuum. For the parameters stated above, the cutoff predicted by the three-step model is at $\Omega = 45\omega_L$.

In [10] a striking agreement between the wavelet transforms for the ground-state-continuum projection and the full acceleration was observed, at the cutoff and for the whole plateau region. These results are in agreement with a computation [23] for a three-dimensional long-range SAE model involving ultrashort pulses, at the cutoff harmonics, and also with the results in [17]. The present results (not shown) for the plateau and cutoff regions are again in agreement with these calculations, showing their generic, potential-independent nature for an effective single-bound-state atom. As in the short-range case adressed in [10], the main wavelet peak corresponds to a return time of about $t = 0.45T$, periodic over $0.50T$. If the high-lying excited states are taken into account, we obtain a spurious peak at $E(t) = E_0$ for the bound-continuum wavelet. This feature is also observed in the next subsection (III C). We regard it as unphysical, since a projection onto a field-free bound-state basis is not a good approximation for the weakly bound states.

C. Deep long-range potential

After discussing harmonic generation for models with just one or two bound states, we now wish to address the question of whether the spectral features observed are present for an atom with more than two strongly bound states.

We consider $\alpha = 0.76$ and $\beta = 1.1$ in the potential (24), resulting in a ground-state energy of $\varepsilon_0 = -0.501$ a.u. This case differs from the one considered in Sec. III B in the sense that also the first and second excited states, of energies, respectively, $\varepsilon_1 = -0.199$ a.u. and $\varepsilon_2 = -0.108$ a.u., are relatively deeply bound and strongly coupled (the dipole matrix elements between the states are, respectively, $\langle 0|x|1\rangle = 1.19$ and $\langle 1|x|2\rangle = 3.02$). The cutoff for this potential is, with the field parameters taken as in Sec. III A, at $\Omega = 49\omega_L$.

In Fig. 4, for the part of the spectrum above the 13th harmonic, we observe a perfect agreement between the spectrum of $\ddot{x}_{bc}(t)$ including the three most deeply bound states (c) and the full acceleration spectrum (a). The inclusion of the higher excited states (b) makes the agreement much worse, indicating the inadequacy of the field-free basis for this intensity regime. The bound-bound transitions involving only the three strongly bound states (d) exhibit a cutoff at a much lower frequency, the term proportional to $E(t)$ in Eq. (2) modifying only the background in this case. The harmonic intensities are much lower than those of the full result. The spectrum of $\ddot{x}_{bb}(t)$ involving *all* the bound states (e) (their number is finite within our discretization) yields a smeared out cutoff, which is also observed by [6]. Moreover, we observe that the spectra corresponding to continuum-ground-state transitions are at least two orders of magnitude higher than bound-continuum spectra involving only the excited bound state parts. The harmonic yields from these contributions decrease with increasing bound-state energy. This is shown in Fig. 4(f), where the contributions from the transitions involving the continuum and the bound state $|2\rangle$ are

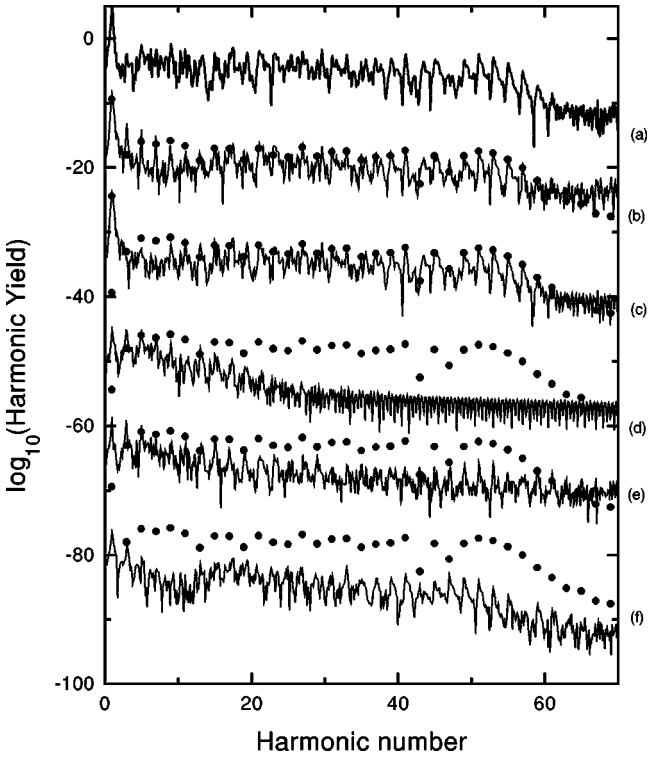

FIG. 4. Power spectra of the time-dependent dipole acceleration for the deep Coulomb potential. (a) full acceleration; (b) bound-continuum part; (c) bound-continuum part from the three most deeply bound states; (d) bound-bound part from the three most deeply bound states; (e) bound-bound part; (f) bound-continuum part for the second excited state only. All subsequent curves have been shifted by -15 y-axis units from their respective upper neighbors. The harmonic peak heights from curve (a) have been repeated as the filled circles for all other five curves, as a point of reference.

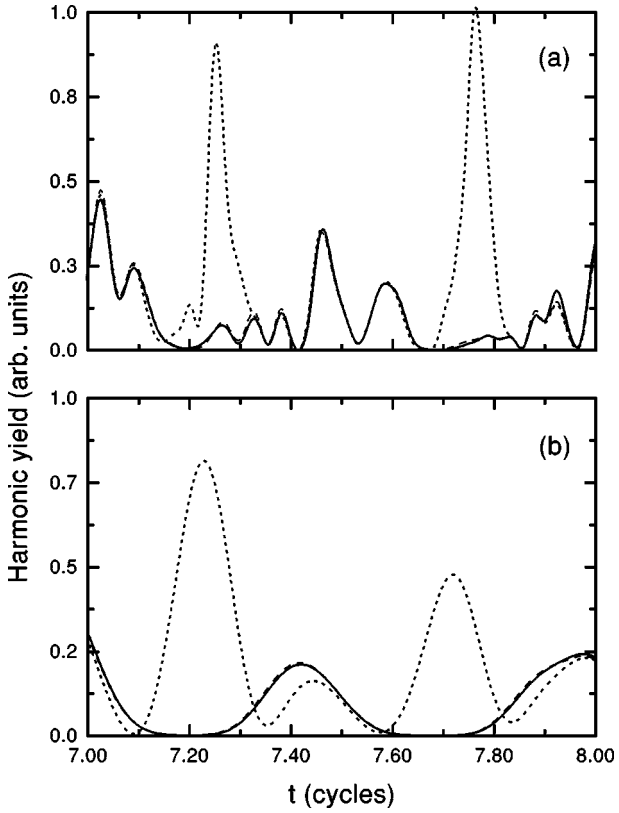

FIG. 5. Wavelet analysis of the time-dependent dipole acceleration over one cycle of the driving laser field for the deep Coulomb potential. (a) Plateau harmonics, $\Omega=37\omega_L$, $\sigma=0.027T$; (b) cutoff harmonics, $\Omega=51\omega_L$, $\sigma=0.108T$. Solid line: full dipole acceleration. Dashed line: bound-continuum contributions from the three most deeply bound states. Dotted line: bound-continuum contributions.

presented. The contributions to the *b*-*c* spectrum from the first excited state $|1\rangle$ are one to two orders of magnitude smaller than those involving the ground state. Similar results were obtained by [24] in a time-dependent computation, in which the initial atomic state was taken as a coherent superposition of the ground and lowest metastable excited state. Indeed, in three-step models for high-harmonic generation the excited bound states are usually neglected, which is justified in view of the present results.

The corresponding wavelet analysis in Fig. 5 shows that the bound-continuum part, which includes only the lowest three bound states, and the full acceleration yield almost indistinguishable wavelet transforms for both (a) and (b). The bound-continuum part including all bound states is also in agreement with the other two sets of results, apart from a spurious peak at maximal field ($t=0.25T$ modulo $0.5T$). This spurious (unphysical) peak is due to the contribution of the high-lying excited states in the time-dependent projections. This peak is not present in the harmonics of energy higher than the cutoff, indicating that it arises only from the high-plateau harmonics. Once more, in part (b), the cutoff return time $t\simeq 0.4T$ is recovered for the full acceleration and $\ddot{x}_{bc}(t)$.

For the lower-energy part of the spectra, however, the harmonics appear to be a ''mixture'' of bound-continuum and bound-bound transitions, and it is difficult to draw conclusions about which mechanism plays the most important role. This is clearly observed in the wavelet transform centered at the 7th harmonic (not shown). In this case, the wavelet transform no longer exhibits the $T/2$ periodicity of the driving field but there are other time scales present, presumably due to resonant processes involving several bound atomic states. Concerning the term in $\ddot{x}_{bb}(t)$, which is proportional to the field, as briefly mentioned in Sec. II A it introduces an overenhancement of the peak at maximum field ($t=0.25T$ modulo $0.5T$) when all the bound states are taken into account. The reason is that the projections on all these states become large for maximal field. If just the three most deeply bound states are taken into account, the term in $E(t)$ plays no important role in the wavelet transforms, the result with and without this term being almost identical. Moreover, even though the excited states $|1\rangle$ and $|2\rangle$ are strongly coupled, the wavelet transform of $\ddot{x}_{bc}(t)$ for only the two or only the three most deeply bound states present no significant difference.

D. Effects of the Coulomb tail

In order to investigate quantitatively the effects of the long-range Coulomb tails in the deep Couomb potential of Sec. III C, we now discuss and compare results obtained with the same potential, where the Coulomb tails have been cut off,

$$V_T(x)=V_C(x)\begin{cases}1, & |x|<a_0\\ \cos^n\left[\dfrac{\pi}{L-a_0}(x-a_0)\right], & a_0<|x|<L\\ 0, & L<|x|.\end{cases} \tag{25}$$

For regions close to the atomic core, this expression yields the deep Coulomb potential V_C from Sec. III C. For $|x|>a_0$, its tails are cut off smoothly. We take $a_0=5$, $n=6$, and $L=2\alpha_0$, α_0 being the excursion amplitude of the electron ($\alpha_0=E_0/\omega^2=32$). Thus within its excursion amplitude, the electronic wave packet will experience a very different potential tail betwee V_C and V_T. For the parameters above, the ground-state energy ε_0 of V_T is the same as the one for V_C (Sec. III C), while the first and second excited states' energies of V_T are at $\varepsilon_1=-0.192$ and $\varepsilon_2=-0.063$. The energies of the higher excited bound states are of course quite different between the two potentials. (Also the matrix element $\langle 1|x|2\rangle$ is very different.) The truncated potential V_T has only a finite number of bound states, seven within our discretization. We apply exactly the same field pulse as for the previous results shown.

The effects of Coulomb tails on harmonic generation spectra have been discussed in several papers before [25]. Mainly, however, these discussions were concerned with elliptically polarized driving fields, investigating harmonic energies close to the ionization energy (''threshold'' harmonics). Unusual ellipticity dependence was observed, whose origin was usually surmised to lie in the dominant effect of excited bound states. Coulomb corrections to the free wave-packet evolution within the context of multiphoton ionization and above-threshold (high photoelectron energy) multiphoton ionization have also been addressed [26], again mainly in the context of elliptical polarization and thus concerned with wave-packet spreading transverse to its principal excursion amplitude. In the present study, we are uniquely concerned with the *longitudinal* spreading of our (1D) wave packet in a linearly polarized laser field. Even within this restricted context, one should expect quantitative differences in the harmonic yield, since the Coulomb tails affect atomic ionization [26] and the spreading of the electronic wave packet.

When comparing the harmonic generation spectra from V_C and V_T, there are no major differences visible on the scale of Fig. 4 (the results for V_T are not shown in the figure). However, there are quantitative differences of about one order of magnitude. The V_T harmonics at the cutoff are slightly (a factor 2 to 3) lower than the V_C harmonics. On the other hand, there are a few groups of harmonics, in the plateau (around the 35th) and at threshold (around the 11th) where the V_T harmonics are about one to two orders of magnitude higher than the V_C harmonics. Again, there is perfect agreement between the full and the $\ddot{x}_{bc}(t)$ high-energy spectra for V_T, where only the lowest three bound states are taken.

We now consider the wavelet transforms for the two sets of results. For the low harmonics, for $\Omega=7\omega_L$ and $\sigma=0.108T$, we observe that the results for V_T are much less structured than the results for V_C. The results for V_T are dominated by a single smooth peak, near $0.25T$, periodic modulo $T/2$, as was the case for the short-range Gaussian potential, discussed in Fig. 3. This suggests that the nonperiodic wavelet yield of V_C for the low harmonics is inherent to the long-range tail of Eq. (24). However, for the potential (25) it is not clear whether the low harmonics are originated by the bound-bound or bound-continuum transitions, since both contributions present well-defined maxima at peak-field times.

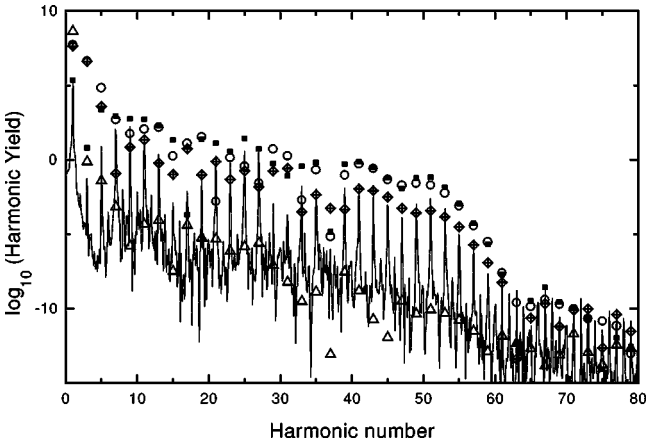

FIG. 6. Power spectra of the dipole acceleration for the Gaussian potential. All projections (but one, see below) are performed in the *velocity* gauge. Solid line: spectrum of the full acceleration (same as in Fig. 1). Filled squares: bound-bound contribution. Circles: bound-continuum contribution. Crossed diamonds: continuum-continuum contribution. Triangles: continuum-continuum contribution from length-gauge projection.

For the plateau region, for $\Omega=37\omega_L$ and $\sigma=0.027T$, V_T again exhibits much less structured temporal profiles than V_C, this time dominated by a peak near $0.50T$. At the cutoff, finally, very similar wavelet yields are obtained for V_T and V_C, once more indicating the potential-independent nature of the cutoff harmonics. The cutoff return time is slightly shifted between the different sets of results: V_C yields $0.42T$, V_T yields $0.47T$, while V_G gave $0.45T$ [10] for the (single) peak of the temporal signal. The width of the peak, however, is much larger than these differences, and thus the wavelet cannot really (neither in practice nor in principle) resolve such a small difference. According to our analysis, the long-range tail of the Coulomb potential influences mainly low- and threshold harmonics, and, depending on the potential in question, might affect particular groups of plateau harmonics. The effect of truncating or not the long-range potential, even quantitatively, does not have a significant influence on the cutoff harmonics.

E. Gauge dependence

As discussed in Sec. II A, the time-dependent projections are gauge-dependent and one has to be careful about the choice of gauge. In the present low-frequency region, the projections make sense only when taken in the length gauge, as has also been argued in [27] and [28]. In this subsection, we present misleading results obtained in the velocity gauge as an example. We take the short-range potential from Sec. III A, which has two deeply bound states, and calculate the time-dependent projections in the velocity gauge. In this case, the plateau- and cutoff-structure is recovered also for

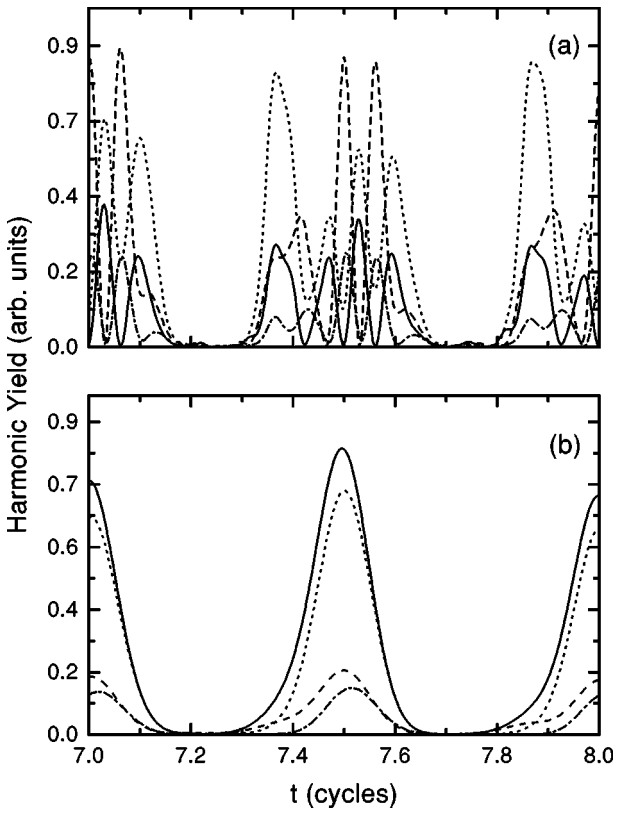

FIG. 7. Wavelet transform of the time-dependent dipole acceleration for the Gaussian potential. The projections are performed in the velocity gauge. (a) Plateau harmonics, $\Omega=37\omega_L$, $\sigma=0.024T$. (b) Cutoff harmonics, $\Omega=49\omega_L$, $\sigma=0.1T$. Solid line: full dipole acceleration. Dashed line: bound-continuum contributions. Dotted line: bound-bound contributions. Dotted-dashed line: continuum-continuum contributions.

the $\ddot{x}_{bb}(t)$ spectrum. This can be seen in Fig. 6, where the spectra for $\ddot{x}_{bb}(t)$, $\ddot{x}_{bc}(t)$, and $\ddot{x}(t)$ in the velocity gauge are presented. The full line gives the ''exact'' result, the same as the dashed line in Fig. 1. The key point of the present figure is that the various projection contributions (bound-bound and bound-continuum) are much larger than the full result (the continuum-continuum contribution is roughly of the order of magnitude of the full result). This indicates that the projections in the velocity gauge cannot be expected to yield much physical information individually, since they cancel each other to a large extent when summed to give the full result.

Moreover, performing the wavelet analysis for the present case, shown in Fig. 7(a) for the plateau harmonics, one observes that the $\ddot{x}_{bb}(t)$ contribution is similar to the full $\ddot{x}(t)$, whereas the $\ddot{x}_{bc}(t)$ wavelet is completely out of phase with the full result. This appears to lead to the conclusion that, for atoms with strongly coupled bound states, the bound-bound transitions play a very important role in the generation of plateau harmonics. However, it must be noted that, as shown in Fig. 7(b), all the contributions (although most prominently the bound-free contribution) reproduce the return time $t\simeq 0.5T$ at the cutoff.

Considering the ground-state and excited-state populations obtained by projecting the velocity-gauge wave function, shown as the thin lines in Fig. 2, the former presents maxima for times $t=0.25T$ modulo $0.5T$, corresponding to maximum field strength $E(t)=E_0$. These results are obviously unphysical, when viewed in a quasistatic field picture. This justifies the gauge transformation introduced in the present analysis. Studies concerning the gauge dependence of time-dependent projections were also performed by [27] within the context of population transfer.

IV. CONCLUSIONS

We wish to draw the following qualitative conclusions on high-harmonic generation, based on the results within our projection method.

There is no significant qualitative influence on either low- or high-harmonic generation from the long-range shape of the potential. In other words, for long-range potentials, the highly excited bound states do not play a significant role. When observing 3D effects, however, as for example in the ellipticity dependence of harmonic generation [25], the potential tails may become important. For atoms with more than one bound state, both the bound-bound and the continuum-bound transitions play a role in the harmonic generation process. The generation of high harmonics corresponds to a three-step physical picture, in which the main contributions within a field cycle correspond to the semiclassical return times, even for long-range potentials. For all the potentials studied, only the bound-free transitions originate a cutoff at the semiclassical energy $|\varepsilon_0|+3.17U_p$. Both spectral and time-frequency analysis demonstrate that the main contributions to high-harmonic generation come from transitions involving the ground state. This shows that the electronic wave packet not only rescatters with the atomic potential, but really recombines to the ground state.

On the other hand, the low harmonics appear to be the result of several mechanisms, depending very much on the potential in question. Our analysis shows that indeed the excited bound states play a significant role in the properties of these lower harmonics, in agreement with the interpretation of some of the results in [25,26].

Specifically, for an atom with only two deeply bound states, the bound-bound transitions play the dominant role in the generation of harmonics at the low-energy side of the plateau. Similar results were also obtained by [7]. However, the plateau and cutoff at $\omega_{10}+3U_P$ reported in this publication are absent in our computation. It should be noted that we do take recombination into account for the amplitudes $C_n(t)$. Only in the velocity gauge, for which the time dependence of the ground- and excited state populations yields unphysical results, are a plateau and a cutoff within this frequency regime observed. The mechanism of harmonic generation in a two-level atom leads to a temporal structure in the low-harmonic generation, which is completely out of phase with the main process of harmonic generation in a spatially extended atom.

In the low-frequency regime we observe strikingly different bound-bound and two-level atom spectra and wavelet transforms. The spectra can be made to appear more similar if one chooses much higher ionization rates in the two-level atom model. This indicates that the high-frequency components in the amplitudes $C_n(t)$ of the bound states from the full solution are very different from the corresponding components in the amplitudes from the two-level atom model,

due to the contribution of the continuum states in the dynamics of the driven atom, even though the dynamics involves primarily only a charge oscillation between the lowest two bound states. A critical influence of the bound-state population transfers on harmonic generation was also observed by [29], as well as ionization-related effects in the bound-state population dynamics.

For the particular case of an atom with only two strongly coupled bound states, we conclude that the low harmonics are not well represented by a two-level atom. Even the insertion of effective ionization rates yields a completely inappropriate model for the low-energy spectral region. As the harmonic frequency increases, the three-step model becomes the appropriate picture for the high-harmonic generation process.

ACKNOWLEDGMENTS

C.F.M.F. was supported by the DAAD and M.D. was supported in part by the Deutsche Forschungs–Gemeinschaft. The authors are grateful to W. Becker, E. Conejero Jarque, and L. Plaja for useful discussions. We are indebted to R. Kopold and W. Becker for suggesting the mechanism of charge oscillation harmonic generation (Sec. III A).

[1] M. Yu. Kuchiev, Pis'ma Zh. Éksp. Teor. Fiz. **45**, 319 (1987) [JETP Lett. **45**, 404 (1987)]; K. C. Kulander, K. J. Schafer, and J. L. Krause, in *Proceedings of the SILAP Conference*, edited by B. Piraux *et al.* (Plenum, New York, 1993); P. B. Corkum, Phys. Rev. Lett. **71**, 1995 (1993).

[2] M. Lewenstein, Ph. Balcou, M. Yu. Ivanov, A. L'Huillier, and P. B. Corkum, Phys. Rev. A **49**, 2117 (1994); P. Salières, A. L'Huillier, Ph. Antoine, and M. Lewenstein, Adv. At., Mol., Opt. Phys. (to be published).

[3] W. Becker, S. Long, and J. K. McIver, Phys. Rev. A **41**, 4112 (1990); **50**, 1540 (1994).

[4] For a review on these experiments, see A. L'Huillier, L.-A. Lompré, G. Mainfray, and C. Manus, in *Atoms in Intense Laser Fields*, edited by M. Gavrila, Advances in Atomic, Molecular and Optical Physics, (Academic, London, 1992).

[5] B. Sundaram and P. Milonni, Phys. Rev. A **41**, 6571 (1990); L. Plaja and L. Roso-Franco, J. Opt. Soc. Am. B **9**, 2210 (1992); A. E. Kaplan and P. L. Shkolnikov, Phys. Rev. A **49**, 6571 (1994); F. I. Gauthey, C. H. Keitel, P. L. Knight, and A. Maquet, *ibid.* **52**, 525 (1995); S. de Luca and E. Fiordilino, J. Phys. B **29**, 3277 (1996).

[6] E. Conejero Jarque and L. Plaja, J. Opt. Soc. Am. B **13**, 2724 (1996).

[7] E. Conejero Jarque and L. Plaja, J. Phys. B **31**, 1687 (1998).

[8] M. Lewenstein, P. Salières, and A. L. Huillier, Phys. Rev. A **52**, 4747 (1995); P. Antoine, M. B. Gaarde, P. Salières, B. Carré, A. L'Huillier, M. Lewenstein, in *Multiphoton Processes 1996*, edited by P. Lambropoulos and H. Walther (IOP Publishing, Bristol, 1997); J. Zhou, J. Peatross, M. M. Murnane, H. C. Kapteyn, and I. P. Christov, Phys. Rev. Lett. **76**, 752 (1996A); P. Salières, T. Ditmire, M. D. Perry, A. L'Huillier, and M. Lewenstein, J. Phys. B **29**, 4771 (1996).

[9] See, e.g., S. C. Rae, K. Burnett, and J. Cooper, Phys. Rev. A **50**, 3438 (1994).

[10] C. Figueira de Morisson Faria, M. Dörr, and W. Sandner, Phys. Rev. A **55**, 3961 (1997).

[11] See, e.g., M. Protopapas, C. H. Keitel, and P. L Knight, Rep. Prog. Phys. **60**, 389 (1997), and references therein.

[12] See, e.g., K. Burnett, V. C. Reed, J. Cooper, and P. L. Knight, Phys. Rev. A **45**, 3347 (1992); J. L. Krause, K. Schafer, and K. Kulander, *ibid.* **45**, 4998 (1992).

[13] See, e.g., C. Leubner and P. Zoller, J. Phys. B **13**, 3613 (1980), and references therein.

[14] L. Allen and J. Eberly, *Optical Resonance and Two-Level Atoms* (Wiley, New York, 1975).

[15] B. W. Shore, *Theory of Coherent Atomic Excitation* (Wiley, New York, 1990).

[16] L. D. Landau and E. M. Lifshitz, *Quantum Mechanics* (Pergamon Press, Oxford, 1977).

[17] See, e.g., P. Antoine, A. L'Huillier, and M. Lewenstein, Phys. Rev. Lett. **77**, 1234 (1996).

[18] F. I. Gauthey, B. M. Garraway, and P. L. Knight, Phys. Rev. A **56**, 3093 (1997).

[19] M. Yu. Ivanov and P. B. Corkum, Phys. Rev. A **48**, 580 (1993); T. Zuo, S. Chelkowski, and A. D. Bandrauk, Phys. Rev. A **48**, 3839 (1993).

[20] R. Kopold and W. Becker (unpublished).

[21] P. Antoine, B. Piraux, and A. Maquet, Phys. Rev. A **51**, R1750 (1995); R. Taieb, A. Maquet, P. Antoine, and B. Piraux, in *Proceedings of the SILAP4 Conference*, edited by H. G. Muller and M. V. Fedorov (Kluwer, 1996); P. Antoine, B. Piraux, D. B. Milosevic, and M. Gajda, Phys. Rev. A **54**, R1761 (1996).

[22] W. Becker, A. Lohr, M. Kleber, and M. Lewenstein, Phys. Rev. A **56**, 645 (1997).

[23] K. J. Schafer and K. J. Kulander, Phys. Rev. Lett. **78**, 638 (1997).

[24] J. B. Watson, A. Sanpera, X. Chen, and K. Burnett, Phys. Rev. A **53**, R1962 (1996); A. Sanpera, J. B. Watson, M. Lewenstein, and K. Burnett, *ibid.* **54**, 4320 (1996).

[25] K. Miyazaky and H. Sakai, J. Phys. B **25**, L83 (1992); K. S. Budil, P. Salières, A. L'Huillier, T. Ditmire, and M. D. Perry, Phys. Rev. A **48**, R3437 (1993); K. Miyazaki, H. Sakai, G. U. Kim, and H. Takada, *ibid.* **49**, 548 (1994); N. H. Burnett, C. Kan, and P. B. Corkum, *ibid.* **51**, R3418 (1995); K. Miyazaki and H. Takada, *ibid.* **52**, 3007 (1995); M. Yu. Ivanov, T. Brabec, and N. Burnett, *ibid.* **54**, 742 (1996); T. Brabec, M. Yu. Ivanov, and P. B. Corkum, *ibid.* **54**, 2551 (1996).

[26] X. Mu, Phys. Rev. A **43**, 5149 (1991); H. R. Reiss and V. P. Krainov, *ibid.* **50**, R910 (1994); J. Z. Kamiński, *ibid.* **37**, 622 (1988); M. H. Mittlemann, *ibid.* **50**, 3249 (1994); M. V. Fedorov and J. Peatross, *ibid.* **52**, 504 (1995); J. Z. Kamiński, A. Jaroń, and F. Ehlotzky, *ibid.* **53**, 1756 (1996); J. Z. Kamiński and F. Ehlotzky, *ibid.* **54**, 3678 (1996); S. F. J. Larochelle, A. Talebpour, and S. L. Chin, J. Phys. B **31**, 1215 (1998).

[27] K. J. Schafer and K. C. Kulander, Laser Phys. **7**, 740 (1997).

[28] S. Vivirito and K. Taylor (private communication).

[29] M. L. Pons, R. Taieb, and A. Maquet, Phys. Rev. A **54**, 3634 (1996).